coatings

MDPI

Article

Structure and High-Temperature Oxidation Performance of Si-Co Diffusion Coatings Prepared on a TiAl-Nb Alloy

Jin Tian [1,2], Conghui Zhang [1,3,*], Wei Lv [4], Xuan Li [4] and Wei Tian [2]

[1] College of Metallurgical Engineering, Xi'an University of Architecture and Technology, Xi'an 710055, China; li19801228@sina.com
[2] China United Northwest Institute for Engineering Design and Research Corporation, Xi'an 710077, China; tianwei830926@sina.com
[3] Shaanxi Science and Technology Agency, Shaanxi International Science and Technology Cooperation Base, Xi'an 710077, China
[4] College of Mechanical Engineering, Sichuan University of Science and Engineering, Zigong 643000, China; chutianxiu@163.com (W.L.); biluaner@163.com (X.L.)
* Correspondence: zhangconghui@xauat.edu.cn; Tel.: +86-180-9129-0108

Abstract: Si-Co diffusion coatings were prepared on a Y-modified TiAl-Nb alloy using the pack cementation process. The structures of the coatings prepared at different temperatures (1050, 1080, and 1120 °C) and pack Co contents (5, 10, and 20 wt.%) were comparatively studied. The coatings possessed the typical structure of a (Ti,*X*)Si_2+Ti_5Si_4 (*X* represents Nb and Al elements) outer layer with a Co-rich superficial zone, a Ti_5Si_4+Ti_5Si_3 middle layer, and a $TiAl_2$ inner layer. Increasing the co-deposition temperature in the range of 1050–1120 °C led to a larger coating thickness but a more-porous coating structure, while increasing the pack Co contents in the range of 5–20 wt.% caused a lower coating growth rate. The formation of the Si-Co diffusion coating followed an orderly process of depositing Si first and then Co. The Si-Co diffusion coating had much better anti-oxidation performance than both the TiAl-Nb substrate and pure silicide coating. After undergoing oxidation at 1000 °C for 100 h, the oxidation parabolic rate of the Si-Co diffusion coating was approximately 6.16×10^{-3} mg^2/cm^4h^1, which was lower than those of the TiAl-Nb substrate by about two orders of magnitude and pure silicide coating by about one order of magnitude.

Keywords: TiAl-Nb alloy; Si-Co co-deposition; coating structure; oxidation; scale formation

check for updates

Citation: Tian, J.; Zhang, C.; Lv, W.; Li, X.; Tian, W. Structure and High-Temperature Oxidation Performance of Si-Co Diffusion Coatings Prepared on a TiAl-Nb Alloy. *Coatings* **2023**, *13*, 1427. https://doi.org/10.3390/coatings13081427

Academic Editor: Hideyuki Murakami

Received: 23 June 2023
Revised: 6 August 2023
Accepted: 9 August 2023
Published: 14 August 2023

Copyright: © 2023 by the authors. Licensee MDPI, Basel, Switzerland. This article is an open access article distributed under the terms and conditions of the Creative Commons Attribution (CC BY) license (https://creativecommons.org/licenses/by/4.0/).

1. Introduction

TiAl alloys have great potential for application in advanced aeroengines and various gas turbines because of their good combination of properties: low density, high specific strength and stiffness, excellent high-temperature mechanical properties, and oxidation resistance [1,2]. Compared with common TiAl alloys, the high-Nb-containing TiAl alloys (TiAl-Nb) possess better oxidation resistance and creep properties under the function of the solid-solution-strengthening and precipitation-phase-strengthening effects of the element Nb [3]. However, for use in hot-end components servicing at temperatures higher than 850 °C, the oxidation resistance of TiAl-Nb alloys is still poor because considerable amounts of less-protective TiO_2 will form in the oxide scale during oxidation [4].

Applying a protective coating is an effective way to improve the oxidation resistance of TiAl alloys. Generally, an ideal anti-oxidation coating for TiAl alloys is expected to form a dense, slow-growing scale, such as $A1_2O_3$, Cr_2O_3, SiO_2 or their composites, to prevent the inward diffusion of oxygen and other contaminants. Various anti-oxidation coatings such as aluminide coatings, TiAlCr(Y) coatings, M-CrAlY (M represents N, Ni, Co or NiCo) coatings, ceramic coatings, silicide coatings, and some composite coatings, prepared by different methods, have been employed on TiAl alloys [5–17]. Among these coatings, aluminide coatings can offer fairly good anti-oxidation performance for TiAl alloys by

forming a dense protective Al_2O_3 scale when oxidized at high temperatures; however, the inter-diffusion of Ti and Al between the coatings and TiAl substrate during the oxidation process will accelerate the degradation of the coatings [6,7]. TiAlCr and M-CrAlY coatings possess good anti-oxidation performance by forming the scales composed of Al_2O_3 and Cr_2O_3 during oxidation, thus they were suitable as the oxidation protective coatings for TiAl alloys to be used at 900–1100 °C [8–11]. Unfortunately, a brittle Cr-rich solid-solution layer is prone to forming in the coating/TiAl interface at high temperatures, which is harmful to the bonding strength of the coatings/substrates [10]. Ceramic coatings have excellent high-temperature oxidation resistance and can hardly degenerate; however, the high brittleness of the coatings themselves, together with the thermal-expansion coefficient mismatch between ceramic coatings and TiAl alloys (the linear-expansion coefficients of TiAl alloys is about 12.0×10^{-6}/K [12]), means that cracking or even peeling easily occurs during the heating and cooling processes [13,14]. Some ceramic coatings with composite structures or layers, such as (Al_2O_3-Y_2O_3)/YSZ, (Al_2O_3-Y_2O_3)/(Pt,Au), overcame the defects existing in traditional ceramic coatings to a certain extent; however, this led to new problems such as a long production cycle, a complex process and/or high costs [15,16].

Silicide coatings possess good thermal stability and high-temperature oxidation resistance. During oxidation, a dense and protective SiO_2 scale with a certain fluidity and self-healing ability can form on silicide coatings [17,18]. Among various silicide coatings, Mo-Si, Nb-Si, and SiC coatings are more suitable for components used in ultra-high temperatures such as refractory metals or C/C composites, because the formation of a dense protective SiO_2 scale on these coatings requires temperatures higher than 1000 °C [19–22]. Moreover, 'pesting' oxidation is prone to occur in Mo-Si and Nb-Si coatings at moderate temperatures of about 550–800 °C, which also hindered their practical application on TiAl alloys [19]. Ti–Si compounds ($TiSi_2$, Ti_5Si_4, Ti_5Si_3) are considered to be suitable high-temperature protective coatings for TiAl alloys, characterized by the following advantages: (1) An SiO_2 and TiO_2 mixed scale with certain protective properties can form at temperatures above 700 °C without 'pesting' [17] and (2) the thermal-expansion coefficients of Ti-Si coatings and TiAl alloys match well (the linear-expansion coefficients of TiAl alloys, $TiSi_2$ and Ti_5Si_3 are about 12.0×10^{-6}/K [12], 10.4×10^{-6}/K [23] and 10.8×10^{-6}/K [24], respectively). Besides TiAl alloys, Ti-Si coatings have also been applied on other titanium alloys such as Ti-6Al-4V- and Ti3Al-based alloys, niobium alloys, nickel-base superalloys, etc. [25–28]. The main drawback of Ti-Si coatings is that a large amount of less-protective TiO_2 will be unavoidably formed in the scale of Ti-Si coatings, as a result of the high activity of titanium [29,30]. Moreover, the external diffusion of titanium during the oxidation process will further increase the content of TiO_2 in the scale, seriously weakening the high-temperature protection performance. Even for $TiSi_2$, which possesses the highest Si content among Ti–Si compounds, the content of TiO_2 in the scale is nearly at 60% after being oxidized at 1100 °C for 1000 h [30]. Thus, promoting the formation of SiO_2 but suppressing the formation of TiO_2 in the scale should be the key aim to improve the high-temperature oxidation performance of Ti–Si compound coatings. The addition of Co, Ni or Cr elements, which were named 'the third elements', has been proven to be effective in inhibiting the formation of TiO_2 in the scale by reducing the content of Ti in the coating [31]. Strydom et al. [29] compared the oxidation behavior of $CoSi_2$, $CrSi_2$, $NiSi_2$, PtSi, $TiSi_2$ and $ZrSi_2$ in the temperature range of 750–1100 °C and found that a dense protective SiO_2 scale was formed on $CoSi_2$, while the scale formed on $TiSi_2$ was mainly composed of SiO_2 and TiO_2 mixtures. Zamoum et al. [32] found that the oxidation-rate constant of $Nb_4Co_4Si_7$ compounds at 1300 °C is only about 6×10^{-13} g^2/cm^4s, revealing the excellent oxidation resistance of Co–Si compounds at high temperatures. The rare earth element yttrium is widely used as a modification element in high-temperature alloys and anti-oxidation coatings due to its reactive element effect (REE) [33]. Intensive studies have proved that the addition of minor yttrium (0.06–0.3 at.%) in titanium alloys can effectively improve their high-temperature oxidation resistance by refining and purifying the structure of the alloys, promoting the formation of a protective oxide film, and enhancing its resistance to stripping [34,35].

In this study, the halide-activated pack cementation technique (HAPC), which is characterized as a low-cost, convenient, and widely used method, was employed to prepare the Si-Co diffusion coatings on a Y-modified TiAl-Nb alloy [24,36]. The structures of the coatings prepared at different co-deposition temperatures and pack Co contents were investigated, based on which the high-temperature oxidation performance of the coating with a proper structure was studied.

2. Materials and Methods

Based on our previous research, a yttrium-modified TiAl-Nb substrate with a composition of Ti45Al-6Nb-0.1Y was prepared by the vacuum-consumable arc-melting method [37]. The raw materials used were titanium sponge, Al and Nb powders with a purity of 99.8%, and Y powders with a purity of 99.6%. All of these materials were supplied by Sinopharm Chemical Reagent Co., Ltd., located in Shanghai, China. Before smelting, the raw materials were sequentially subjected to degreasing, acid cleaning, alkali cleaning, and alcohol cleaning to remove their surface oxides and contaminants. A self-made high-temperature, high-vacuum water-cooled crucible arc-melting furnace, equipped with a tungsten rod (arc gun) as the cathode and a copper crucible as the anode, was employed for re-melting the ingot. During smelting, high-purity argon gas was introduced to fill the furnace, to prevent the oxidation of highly active elements such as Ti, Al, and Y, and to suppress the volatilization of low-melting-point elements of Al. To minimize the component segregation, each alloy component was re-melted three times.

The microstructure and XRD pattern of the yttrium-modified TiAl-Nb ingot are shown in Figure 1. From the SEM and TEM-BF images in Figure 1a,b, it is seen that the ingot is mainly composed of three distinctive phases. The XRD pattern of the ingot shown in Figure 1c reveals the formation of α_2-$TiAl_3$, γ-TiAl and B_2 phases in the ingot, which is also confirmed by the diffraction patterns of the different phases shown in Figure 1d–f. Through a comprehensive analysis of the microstructure images, the XRD pattern, and the diffraction patterns of the different phases in the ingot, the Ti45Al-6Nb-0.1Y ingot should be mainly composed of α_2-$TiAl_3$+γ-TiAl lamellar, γ-TiAl and B_2 phases. It is noted that no Y-containing phase was found in the alloy, mainly because the trace Y in TiAl-Nb alloys tends to dissolve in the grain boundary region of the alloy [38].

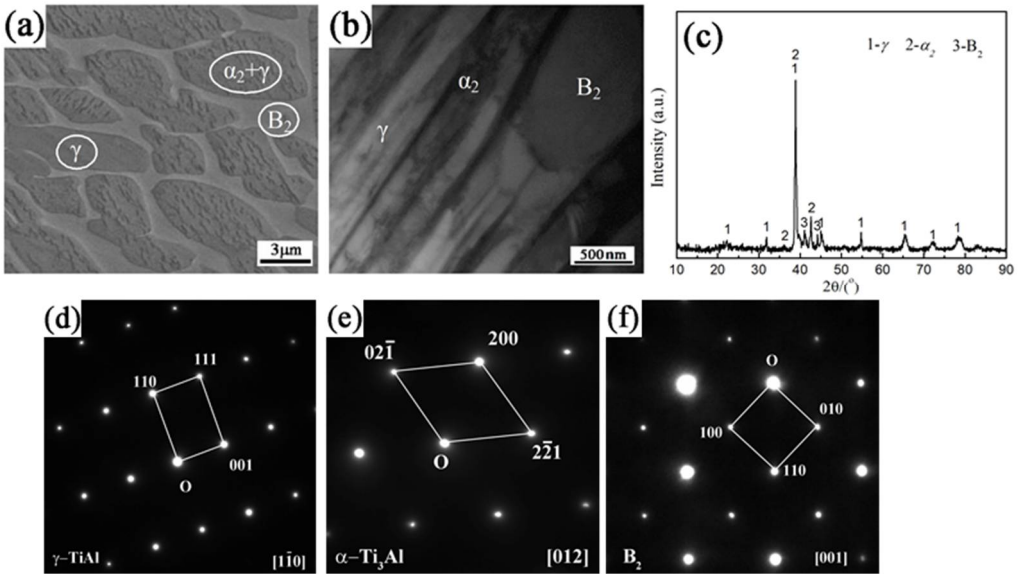


Figure 1. Microstructure images and XRD pattern of the Ti45Al-8Nb-0.3Y alloy. (**a**) SEM image, (**b**) TEM-BF image, (**c**) XRD pattern and the diffraction patterns of the phases (**d**) γ-TiAl, (**e**) α_2-$TiAl_3$, and (**f**) B_2.

The specimens to be coated were cut from the ingot into cuboids measuring 10 mm × 10 mm × 4 mm. Before packing, each surface of the specimens was polished using 1000 # SiC paper and then ultrasonically cleaned in an acetone bath. According to the previous research of our team [37], NaF was a proper activator for Si-Co co-deposition on TiAl alloys, thus the Si-Co diffusion coatings were prepared using pack powders of 20Si-(5-15)Co-5NaF-(60-70)Al_2O_3 (wt.%) in this paper. In the pack powders, Si and Co powders with a purity of 99.8% were utilized as the donor sources, NaF powder with a purity of 99.9% was utilized as the activator, and Al_2O_3 powder with a purity of 99.9% was utilized as the filler. All the powders were produced by Sinopharm Chemical Reagent Co., Ltd. in Shanghai, China, and they had a particle size of 200 mesh. The total weight of the pack powders utilized for each sample was 50 g. Before packing, the powders were ball-milled in a planetary ball mill to be fully mixed and refined. Each sample to be coated was buried nearly in the center of the pack powders contained in an alumina crucible with a capacity of 50 mL, which was then sealed with Na_2SiO_3. The deposition temperature was chosen as 1050, 1080, and 1120 °C, and the holding time was 6 h. The furnace was heated to the intended temperature at a rate of 16 °C/min. After coating, each face of the samples was slightly brushed and then ultrasonically cleaned in an acetone bath to remove the residual pack powders. Pure silicide coatings, which were used as the comparison samples, were also prepared with the pack powders of 20Si-5NaF-75Al_2O_3 (wt.%), using the same pack parameters and processes mentioned above.

The high-temperature oxidation tests of the TiAl–Nb substrate, the pure silicide coating, and the Si-Co diffusion coatings were performed in an electric furnace at 1000 °C in air. The mass changes the specimens after oxidation were measured by an electronic balance with an accuracy of 0.01 mg.

X-ray diffraction (XRD, Panalytical X'Pert PRO, Cu Kα, 50 kV, 200 mA, Etten Leur, The Netherlands) was employed to identify the constituent phases of the ingot, the coatings and their oxides, with a step size of 0.033°/s and a diffraction angle (2θ) ranging from 10° to 90°. The microstructure of the ingot was examined by a scanning electron microscope (SEM, JSM-6360LV, JEOL, Akishima-shi, Japan) equipped with an energy dispersive spectroscope (EDS) and a transmission electron microscope (TEM, Tecnai F30 G2, Hillsboro, OR, America). The microstructure and compositions of the coatings and their oxidation scales were examined by scanning electron microscopy (SEM, JSM-6360LV) and energy dispersive spectroscopy (EDS).

3. Results

3.1. Coating Structures

3.1.1. Effects of Co-Deposition Temperatures

Figure 2 shows the cross-sectional BSE images and elemental concentration profiles of the Si-Co diffusion coatings prepared at 1050, 1080, and 1120 °C for 6 h, respectively, using pack powders of 20Si-10Co-5NaF-65Al_2O_3 (wt.%). Figure 3a presents the surface XRD patterns of the coatings prepared at different co-deposition temperatures, and Figure 3b shows the XRD pattern of the outer layer of the coating prepared at 1080 °C for 6 h.

From the cross-sectional images in Figure 2a–c, it is seen that the Si-Co diffusion coatings prepared at these temperatures possess similar multi-layer structures. However, the coating thickness increased significantly with the increase of the co-deposition temperature, indicating the promoting effects of higher co-deposition temperatures on the coating's growth rate. It is also noted that intensive holes and micro-holes formed in the coating prepared at the highest co-deposition temperature of 1120 °C. The solid-state diffusion coefficient can be described as having an exponential relationship with the temperature. A higher co-deposition temperature means higher inward diffusion rates of Si and Co atoms and led to a larger coating thickness. However, a higher co-deposition temperature also means the more-rapid consumption of pack Si resources in the pack, resulting in the deficiency of Si atoms in the later co-deposition stage, and finally producing a more-porous coating structure.

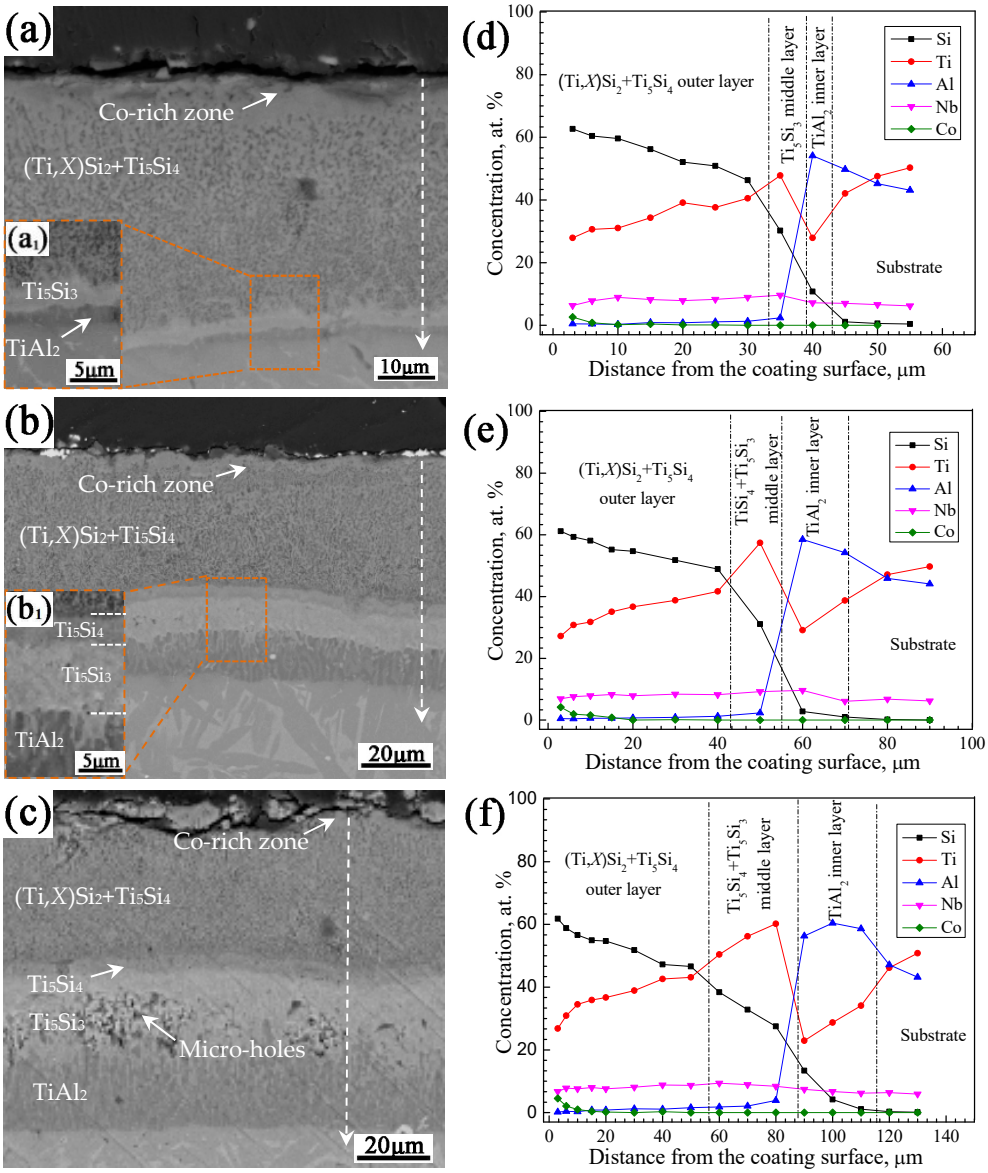


Figure 2. Cross-sectional BSE images (**a**–**c**) and elemental concentration profiles (**d**–**f**) of the Si-Co diffusion coatings prepared at 1050–1120 °C using pack powders of 20Si-10Co-5NaF-65Al2O3 (wt.%). (**a**,**d**) 1050 °C, (**b**,**e**) 1080 °C, and (**c**,**e**) 1120 °C. (**a**$_1$,**b**$_1$) Morphologies of the designated areas of the corresponding coatings under high magnification.

The EDS analysis results in Figure 2b–f reveal that the outer layers of the coatings prepared at different temperatures possess Si content higher than 45 at.% and a relatively higher Co concentration in their superficial zones (higher than 2.6, 4.2, and 4.5 at.% for the coatings prepared at 1050, 1080, and 1120 °C, respectively). Combined with the XRD patterns in Figure 3a,b and the binary phase programs of Ti-Si [39] and Co-Si [40], the outer layers of the coatings prepared at these temperatures can be determined as (Ti,*X*)Si_2+Ti_5Si_4 mixtures (*X* represents Nb and Al elements), in which small amount of a $CoSi_2$ phase formed in the superficial zones. It noted that some $CoSi_2$ diffraction peaks can be observed in the surface XRD patterns (Figure 3a) but disappeared after stripping the coating by about 15 μm from the surface. This also indicates that the Co-containing phase only exists in the superficial zone of the coating. In addition, some Al_2O_3 diffraction peaks can also be found in the surface XRD patterns of the coatings, as shown in Figure 3a, and this should be caused by the adhered Al_2O_3 particles from the pack powders.

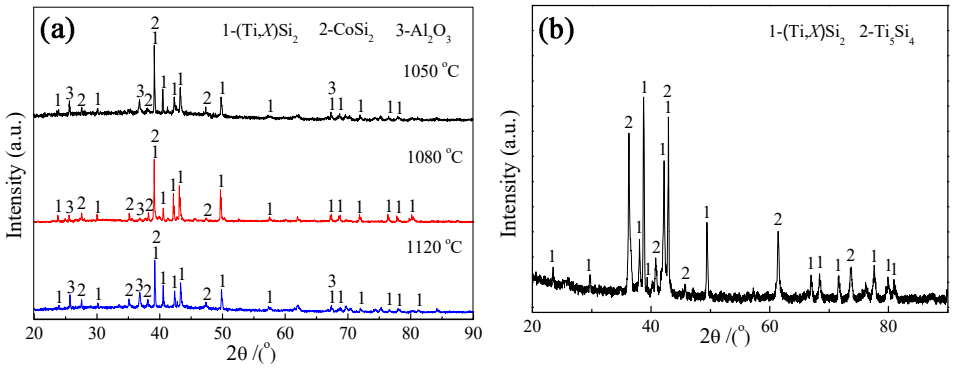


Figure 3. XRD patterns of the Si-Co co-deposition coatings prepared at different temperatures using pack powders of 20Si-10Co-5NaF-65Al_2O_3 (wt.%). (**a**) Surface XRD patterns, (**b**) XRD patterns of the outer layer of the coating prepared at 1080 °C for 6 h, which was obtained after stripping the coating from its original surface by about 15 μm.

The middle layers of the coatings prepared at different temperatures possessed different structural characteristics. For the coating prepared at 1050 °C, as shown in Figure 2(a,a_1), the middle layer has a typical composition of 47.8Ti-30.2Si-2.4Al-9.6Nb (at.%), thus it can be determined as a layer consisting of Ti_5Si_3 [40]. For the coatings prepared at 1080 and 1120 °C, their middle layers mainly consisted of two distinctive parts, as shown in Figure 2(b,b_1,c). EDS analysis revealed that the grey outer parts of the middle layers have a typical composition of 41.7Ti-48.9Si-1.2Al-8.2Nb (at.%), and the light-grey inner parts have a typical composition of 57.4Ti-31.1Si-2.3Al-9.2Nb (at.%). Combined with the Ti-Si binary phase program [40], the outer parts of the middle layers can be determined as Ti_5Si_4 and the inner parts can be determined as Ti_5Si_3.

The inner layers of the coatings prepared at different temperatures have a typical composition of 29.1Ti-2.8Si-58.5Al-9.6Nb (at.%), for which the ratio of the total contents of Ti and Nb atoms to the content of Al atoms is nearly 1:2. According to the Ti-Al-Nb ternary phase diagram by Chen et al. [41], the inner layers of the coatings are composed of the $TiAl_2$ phase (Nb atoms always occupy the lattice position of Ti atoms in Ti-Al-Nb alloys [42]). It is noted that the thinner the total coating thickness, the thinner the $TiAl_2$ inner layer. This should be mainly caused by the low solid solubility of Al atoms in titanium-silicides (lower than 3 at.% in Ti_5Si_3 at 900 °C [43]), which means that Al atoms were gradually being pushed into the substrate to form the $TiAl_2$ inner layer with the inward growth of the Ti_5Si_3 layer. Clearly, less overall coating thickness means less Al atoms are pushed, resulting in a thinner $TiAl_2$ inner layer.

3.1.2. Effects of Pack Co Contents

The observations in Section 3.1.1 revealed that the coating prepared at 1080 °C for 6 h is relatively dense and possesses a proper coating thickness. Thus, the effects of pack Co contents on the coating structures were investigated at the co-deposition temperature of 1080 °C. Figure 4 shows the cross-sectional BSE images and elemental concentration profiles of the Si-Co diffusion coatings prepared with 5 and 15 wt.% Co powders in the pack, in combination with the coating prepared with 10 wt.% pack Co content shown in Figure 2b,d. It is seen that increasing pack Co content led to an obvious suppression effect on the coating's growth rate, as the coating thickness decreased significantly with the increase of pack Co contents.

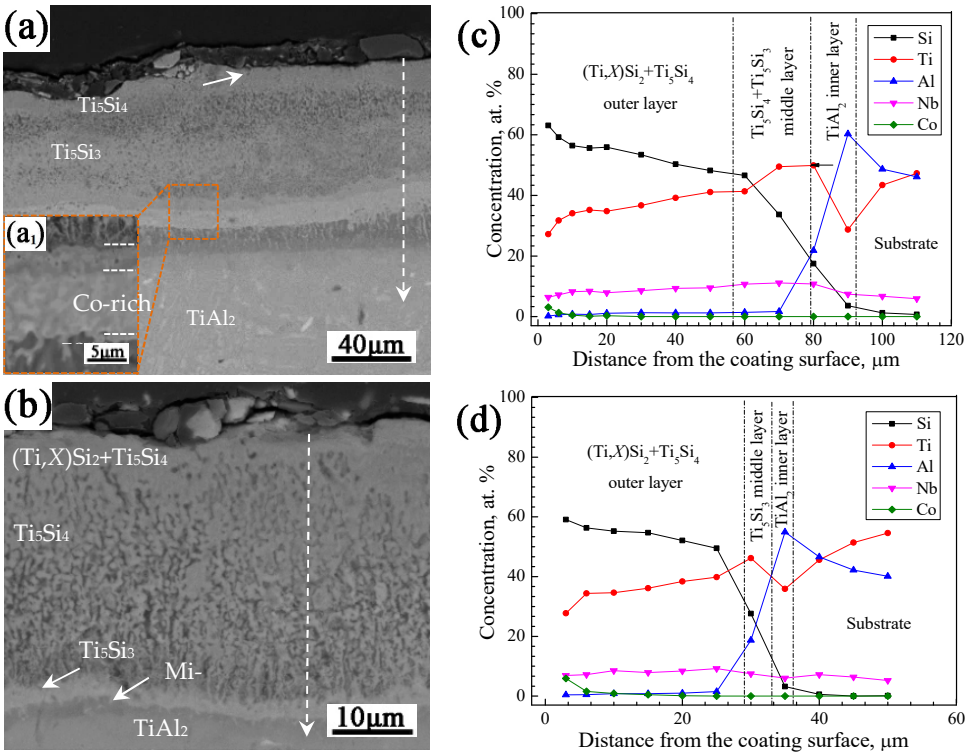


Figure 4. Cross-sectional BSE images (**a**,**b**) and elemental concentration profiles (**c**,**d**) of the Si-Co diffusion coatings prepared at 1080 °C for 6 h using different pack Co contents. (**a**,**c**) 5 wt.%, (**b**,**d**) 15 wt.%. (**a$_1$**) Morphology of the designated area of the corresponding coating under high magnification.

From Figure 4a,c, it is seen that the coating prepared with 5 wt.% pack Co content has a thickness of about 95 μm and possesses a multi-layer structure similar to the coating prepared with 10 wt.% pack Co content: a (Ti,*X*)Si_2+Ti_5Si_4 outer layer with a Co-rich superficial zone, a middle layer consisting of a Ti_5Si_4 outer part and Ti_5Si_3 inner part, and a $TiAl_2$ inner layer. A higher pack Co content of 15 wt.% resulted in a higher Co content of 5.9 at.% in the superficial zone of the coating, but it led to a much lower coating thickness of about 36 μm and a more-porous coating structure, as shown in Figure 4b. In addition, the middle of the coating prepared with 15 wt.% pack Co content is mainly composed of a single Ti_5Si_3 phase (without Ti_5Si_4), which should be caused by the suppression effect of pack Co on the coating's growth rate.

3.2. Coating Formation Process

Generally, the formation process of the coating prepared by pack cementation mainly involves two interrelated processes. One is the process of chemical reactions between the deposition elements and the activator, which generate deposition halide vapors of SiF_x (x = 1, 2, 3, 4) and CoF_y(y = 1, 2, 3). Driven by the chemical gradients between the pack and the substrate surfaces, these vapors species migrated to the surfaces of the substrate alloy and then underwent displacement (Equations (1) and (2)) and disproportionation reactions (Equations (3) and (4)) to release the active atoms [44]. It should be noted that since the standard formation enthalpy of the metal halides is essentially negative within the temperature range applied in this paper, the decomposition reactions of these metal halides can be ignored.

$$SiF_x\ (gas) + Ti\ (s) \rightarrow [Si]\ (solid) + TiF_x\ (gas) \quad (1)$$

$$CoF_y(g) + Ti\ (gas) \rightarrow [Co]\ (solid) + TiF_y\ (gas) \quad (2)$$

$$(x + 1)SiF_x\ (gas) \rightarrow [Si]\ (solid) + xSiF_{(x+1)}\ (gas) \quad (3)$$

$$(x + 1)CoF_y\ (gas) \rightarrow [Co]\ (solid) + yCoF_{(x+1)}\ (gas) \quad (4)$$

Another process mainly involves the inward diffusion of the deposition atoms in the substrate through diffusion or reactive diffusion at high temperatures (solid-state diffusion), which was also considered an important factor to maintain the activity gradient for gas transportation in the pack [36,45]. During this process, the partial pressures of the gas-phase halides of the pack elements will play an important role by affecting the gaseous diffusion. Table 1 lists the standard Gibbs formation energies and the partial pressures of halide Si and Co gases in the pack at 1050, 1080, and 1120 °C, calculated according to the mass conservation law and state equation. It can be seen that the standard Gibbs formation energies of cobalt fluorides are generally higher than those of the silicon fluorides, and the partial pressures of the cobalt fluorides are accordingly lower than those of the silicon fluorides. Such a result revealed that the active Co atoms produced on the substrate surfaces were less than the active Si atoms, and this can be taken as an important factor for the lower content of Co in the diffusion coatings. Fortunately, the difference between the partial pressures of the cobalt fluorides and silicon fluorides is in a reasonable range, which provided an important thermodynamic basis for the successful co-deposition of Si and Co.

Table 1. Calculated standard Gibbs formation energies and partial pressures of the vapor species at 1050, 1080, and 1120 °C.

Species	$\Delta_f G$/(kJ/mol)			Partial Pressures/MPa		
	1050 °C	1080 °C	1120 °C	1050 °C	1080 °C	1120 °C
SiF	−308.9	−314.8	−322.4	4.6×10^{-11}	1.1×10^{-10}	8.9×10^{-9}
SiF_2	−627.8	−628.5	−629.5	5.4×10^{-6}	7.6×10^{-5}	1.3×10^{-5}
SiF_3	−684.8	−683.9	−682.6	4.3×10^{-9}	5.2×10^{-8}	6.5×10^{-7}
SiF_4	−713.0	−710.8	−707.9	9.3×10^{-5}	1.8×10^{-5}	4.4×10^{-4}
CoF	−146.8	−152.0	−160.0	8.2×10^{-10}	2.3×10^{-9}	3.6×10^{-8}
CoF_2	−411.7	−412.8	−414.1	9.4×10^{-7}	1.4×10^{-7}	4.3×10^{-6}
CoF_3	−344.3	−345.1	−345.7	5.5×10^{-8}	7.9×10^{-7}	2.1×10^{-7}

For the solid-state diffusion process, the inward diffusion and reactive diffusion of active Si and Co atoms in the substrate became the dominant factor for the coating's growth. In view of the active atom's inward diffusion, the atom radius and melting point of the pack elements are considered the main affective aspects for the growth of the coating. Although the atom radius and milting point of Co are higher than those of Si, the difference is limited. Thus, the inward solid-state diffusion of Si and Co atoms should be mainly affected by their reactivity with the TiAl-Nb substrate under the fixed temperature. Figure 5 presents the calculated results of the formation energies for Si and Co acting with Ti and Al to form their corresponding compounds at the co-deposition temperatures of 1050, 1080, and 1120 °C. It is seen that the standard Gibbs formation energies of Ti_5Si_3 are the lowest among the possible compounds, followed by Ti_5Si_4 and $TiSi_2$, while those of the Co–Si or Co–Al compounds have relatively higher values (the ΔG values were calculated by the software HSC Chemistry 6.0). Therefore, Ti_5Si_3 would preferentially form during the initial co-deposition period (Equation (5)) and then continuously advance into the substrate. On the contrary, Co–Si or Co–Al compounds can hardly form during the initial coating-formation period.

$$5Ti + 3Si = Ti_5Si_3;\ (1080\ ^\circ C) \approx -588.6\ kJ/mol \quad (5)$$

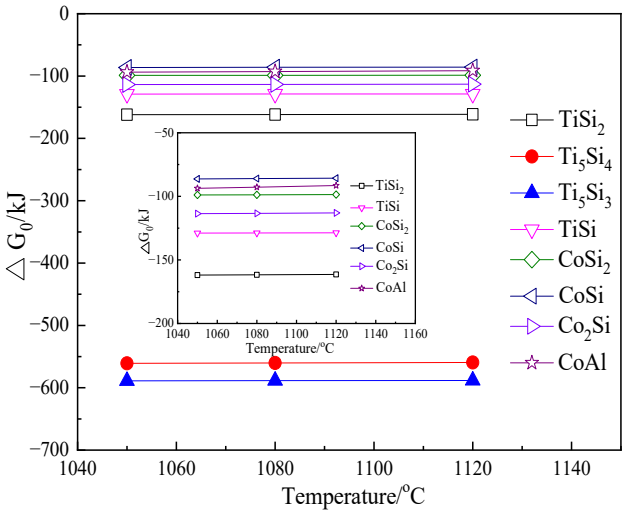


Figure 5. The calculated free-energy changes for Si and Co acting with Ti and Al to form 1 mole of their corresponding compounds at the co-deposition temperatures of 1050, 1080, and 1120 °C.

After the Ti_5Si_3 layer is formed on the substrate, Ti_5Si_4 and $TiSi_2$ would form in sequence through Equations (6) and (7), with Si atoms continuously absorbed on the substrate surface. The formation of the $TiSi_2$+Ti_5Si_4 outer layer in Figures 2 and 4 was the result of these reactions. It is worth noting that the cobalt–silicide compounds such as Co_2Si, CoSi, and $CoSi_2$ can hardly form during this period because the Gibbs formation energies of Co reacting with Ti_5Si_3 or Ti_5Si_4 to form these compounds have positive values, universally higher than 200 kJ/mol, at the employed co-deposition temperatures (calculated using HSC 6.0 software). However, once the $TiSi_2$ outer layer is formed, the formation of cobalt–silicide compounds through Equations (8)–(10) became possible.

$$Ti_5Si_3 + Si = Ti_5Si_4;\ \Delta G_{Ti_5Si_4}\ (1080\ ^\circ C) \approx -92.4\ kJ/mol \quad (6)$$

$$Ti_5Si_4 + Si = TiSi_2;\ \Delta G_{TiSi_2}\ (1080\ ^\circ C) \approx -43.9\ kJ/mol \quad (7)$$

$$TiSi_2 + 4Co = 2Co_2Si + Ti;\ \Delta G_{Co_2Si}\ (1080\ ^\circ C) \approx -62.8\ kJ/mol \quad (8)$$

$$Co_2Si + Si = 2CoSi;\ \Delta G_{CoSi}\ (1080\ ^\circ C) \approx -29.4\ kJ/mol \quad (9)$$

$$CoSi + Si = 2CoSi_2;\ \Delta G_{CoSi_2}\ (1080\ ^\circ C) \approx -12.8\ kJ/mol \quad (10)$$

The above analysis revealed that the formation process of the Si-Co diffusion coatings on the TiAl-Nb alloy actually followed an orderly process of depositing Si first and then Co, during which the inward reaction diffusion of Si in the substrate was the dominant factor for the growth of the diffusion coatings. Such a mechanism can well explain the formation of Co-rich superficial zones in the Si-Co diffusion coatings shown in Figures 2 and 4, which can also explain the suppressed effect of pack Co content on the coating's growth rate, as was found in Section 3.1.2. That is, an increase in pack Co content led to an increase in the adsorption of active Co atoms on the substrate surfaces and correspondingly reduced the adsorption of active Si atoms; as a result, this reduced the growth rate of the coatings.

3.3. Isothermal Oxidation Performance

3.3.1. Oxidation Kinetics

The Si-Co diffusion coating prepared at 1080 °C for 6 h using the pack powders of 20Si-10Co-5NaF-65Al_2O_3 (wt.%) possesses a relatively dense structure and proper thick-

ness, thus this coating was chosen for oxidation tests. The oxidation tests of the TiAl-Nb substrate and pure silicide coating were also carried out for comparison.

Figure 6 shows the isothermal oxidation kinetics of the base alloy, the pure silicide coating, and the Si-Co diffusion coating at 1000 °C, and the macrographic morphologies of the specimens after oxidation at different times are presented simultaneously. It is seen that serious scale spallation occurred on the TiAl-Nb substrate after oxidation for 50 h, while the scale of both the pure silicide coating and Si-Co co-deposition coating remained integrated. After oxidation for 100 h, the Si-Co diffusion coating remained integrated, but obvious spallation occurred at the edges of the pure silicide coating. The above observations revealed the much-better oxidation resistance of the Si-Co diffusion coating than both TiAl-Nb substrate and pure silicide coating.

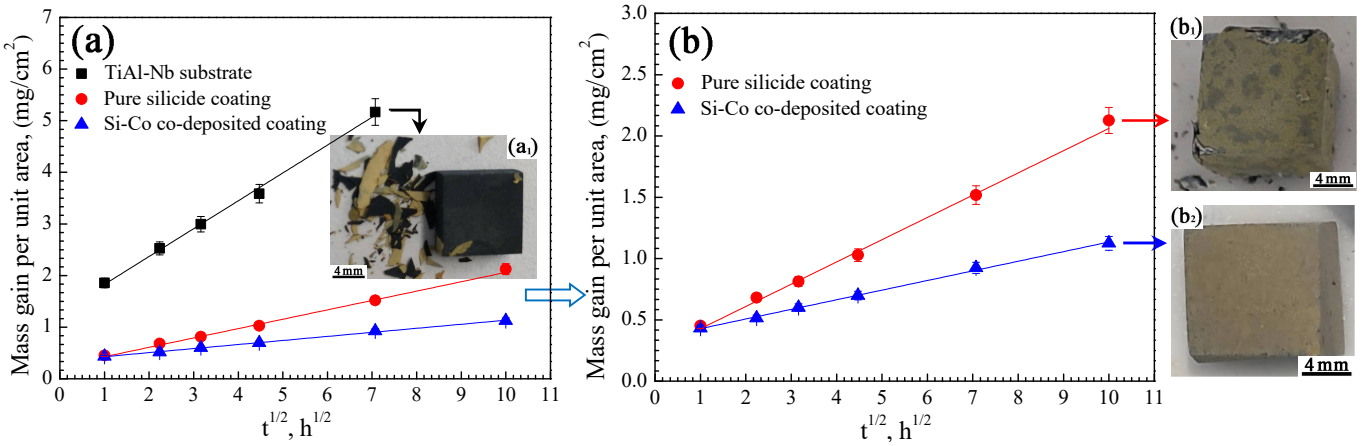


Figure 6. Oxidation kinetics (**a**,**b**) and macrographic morphologies (**a$_1$**,**b$_1$**,**b$_2$**) of the TiAl-Nb substrate, pure silicide coating, and Si-Co diffusion coating at 1000 °C. (**a$_1$**) TiAl-Nb substrate after oxidation for 50 h, and (**b$_1$**) pure silicide coating and (**b$_2$**) Si-Co diffusion coating after oxidation for 100 h.

Based on the mass gains in Figure 6, Table 2 lists the fitted linear equations and parabolic-rate constant (k_p) of the specimens oxidized at 1000 °C for 100 h. It is obvious that the Si-Co diffusion coating possesses a far slower oxidation rate than both the TiAl-Nb substrate and pure silicide coating. Specifically, the Si-Co diffusion coating possesses an oxidation parabolic rate of about 6.16×10^{-3} mg^2/cm^4h^1, which was lower than those of the TiAl-Nb substrate by about two orders of magnitude and pure silicide coating by about one order of magnitude. The above observations once again confirmed the much-better oxidation resistance of the Si-Co diffusion coating than both the TiAl-Nb substrate and pure silicide coating.

Table 2. Fitted linear equations and parabolic-rate constant (k_p) of the TiAl-Nb substrate, pure silicide coating, and Si-Co diffusion coating oxidized at 1000 °C.

Specimens	Fitted Linear Equation	k_p ($mg^2cm^{-4}h^{-1}$)	Correlation Coefficient/R
TiAl-Nb substrate	$y = 1.290 + 0.5396\ t^{1/2}$	2.9×10^{-1}	0.995
Pure silicide coating	$y = 0.246 + 0.1816\ t^{1/2}$	3.30×10^{-2}	0.994
Si-Co co-deposition coating	$y = 0.3497 + 0.0785\ t^{1/2}$	6.16×10^{-3}	0.997

3.3.2. Scale Morphologies

Figure 7 shows the surface and cross-sectional BSE images of the scales formed on pure silicide coating and Si-Co diffusion coating after oxidation at 1000 °C for 100 h, and Figure 8 presents their surface XRD patterns. Table 3 lists the compositions of the typical phases in the scales.

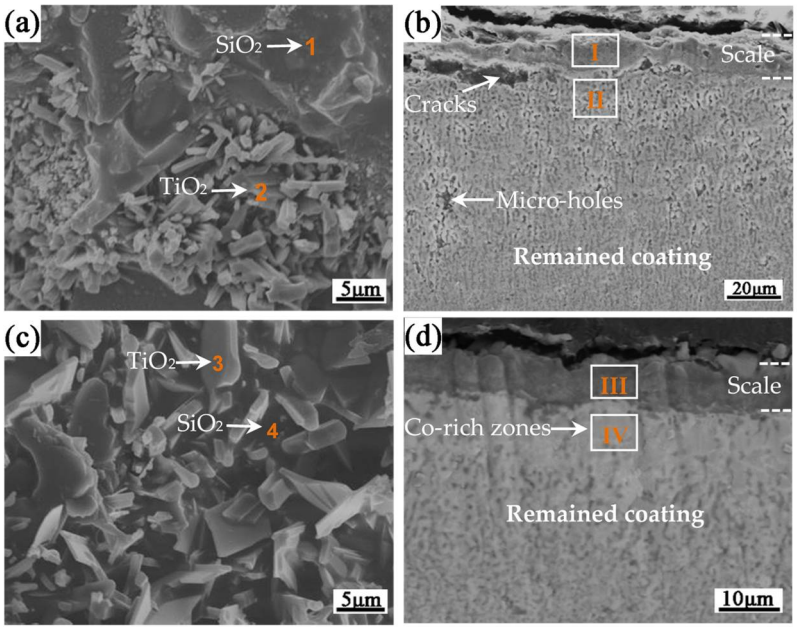


Figure 7. Surface and cross-sectional BSE images of the scales formed on (**a**,**b**) the pure silicide and (**c**,**d**) Si-Co diffusion coatings after oxidation at 1000 °C for 100 h. (**a**,**c**) Surface images, (**b**,**d**) cross-sectional images.

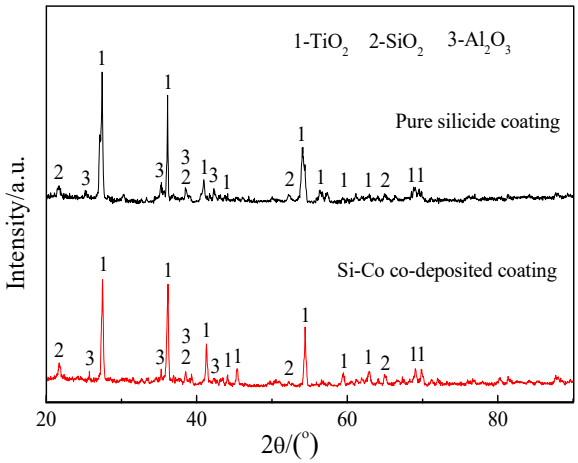


Figure 8. Surface XRD patterns of the scales formed on pure silicide and Si-Co diffusion coatings after oxidation at 1000 °C for 100 h.

Table 3. Composition of the points or areas in Figure 7, determined by EDS analysis.

Points/Areas	Composition (at.%)					
	Si	Ti	Al	Nb	Co	O
1	22.3	5.2	2.6	2.1	/	67.8
2	3.6	23.3	3.4	2.8	/	66.9
3	24.2	3.4	3.2	1.5	0.3	67.4
4	4.2	21.9	3.6	2.0	0.8	67.8
I	11.2	12.7	7.1	1.9		67.1
II	44.8	39.6	1.9	13.7	/	/
III	13.0	9.5	8.2	2.1	0.5	66.7
IV	47.1	32.6	1.6	11.3	7.4	/

From the surface images in Figure 7a,c, the surface XRD patterns in Figure 8, and the EDS analysis results in Table 3, it is seen that the scales of both the pure silicide coating and Si-Co diffusion coating are mainly composed of SiO_2, TiO_2, and Al_2O_3. Of these, the dark matrix was determined to be SiO_2, while the light-grey tissues were determined as TiO_2. The cross-sectional images in Figure 7b,d show that the scale formed on the Si-Co diffusion coating is much denser than the scale formed on the pure silicide coating. The mapping EDS analysis results (areas 'I' in Figure 7b and 'III' in Figure 7d) also confirmed that the scales formed on both the pure silicide coating and the Si-Co diffusion coating consisted of SiO_2, TiO_2, and Al_2O_3 mixtures. The presence of Al_2O_3 in the scale reveals that an outward diffusion of Al occurred during oxidation because the content of Al in the outer layers of both the pure silicide coating and Si-Co diffusion coating is rather low, as confirmed by Figures 2 and 4.

Beneath the scales, there are remaining coatings with compositions of 39.6Ti-44.8Si-1.9Al-13.7Nb (at.%) for the pure silicide coating (area 'II' in Figure 7b) and 32.6Ti-47.1Si-1.6Al-11.3Nb-7.4Co (at.%) for the Si-Co diffusion coating (area "IV' in Figure 7d, confirming that both of them are mainly Ti_5Si_4). The contents of Nb or Co in the remaining coatings are much higher than those in the coatings before oxidation. It is also seen that cracks and intensive Kirkendall holes formed beneath the scale or inside the remaining pure silicide coating, while the remaining Si-Co diffusion coating remained dense and compact. The above findings clearly revealed the better anti-oxidation performance of the Si-Co diffusion coating than the pure silicide coating.

3.3.3. Discussion

At the beginning of oxidation, the coating surface is in direct contact with oxygen at a high temperature, thus the chemical reactions of Equations (11)–(15) were the main factors affecting the growth of scale on the coating surfaces:

$$Si + O_2 = SiO_2,\ \Delta G_{SiO_2}\ (1000\ ^\circ C) \approx -683.2\ kJ/mol \quad (11)$$

$$Ti + O_2 = TiO_2,\ \Delta G_{TiO_2}\ (1000\ ^\circ C) \approx -714.2\ kJ/mol \quad (12)$$

$$2Co + O_2 = 2CoO,\ \Delta G_{CoO}\ (1000\ ^\circ C) \approx -145.6\ kJ/mol \quad (13)$$

$$2Nb + O_2 = 2/5Nb_2O_5,\ \Delta G_{Nb_2O_5}(1000\ ^\circ C) \approx -539.6\ kJ/mol \quad (14)$$

$$4/3Al + O_2 = 2/3Al_2O_3,\ \Delta G_{Al_2O_3}(1000\ ^\circ C) \approx -846.7\ kJ/mol \quad (15)$$

From the calculated free-energy changes of Si, Ti, Co, Nb, and Al reacting with 1 mole of oxygen to form SiO_2, TiO_2, CoO, Nb_2O_5, and Al_2O_3 at 1000 °C in Equations (11)–(15), it is seen that the formation of each oxide is possible without considering the interaction between these elements. Strydom et al. [30] have found that the formation of a single SiO_2 scale on metal-disilicides requires a thermodynamic basis—that the formation energies of the metal oxides are higher than that of SiO_2. Thus, a single SiO_2 scale can hardly form on both the pure silicide coating and the Si-Co diffusion coating due to the lower formation energies of TiO_2 and Al_2O_3 than that of SiO_2. In other words, TiO_2 was the main competitor for the formation of SiO_2 during the initial oxidation period (the influence of Al_2O_3 has been ignored here for its rather low content in the coating surface). In such a situation, the addition of Co with low oxygen affinity in the coating was beneficial for the formation of the SiO_2 in the scale in the initial oxidation stage, as Co is prone to occupying the lattice of Ti atoms in titanium-silicide coatings [46]. A protective initially formed scale can effectively reduce the internal oxidation at the scale/remaining coating interface by suppressing the inward diffusion of oxygen, and thus is beneficial to the adhesion properties of the scale.

Once the protective scale was established, the inward oxygen transport through the scale became difficult, and the oxidation process entered a steady-state period mainly involving the diffusion or inter-diffusion of coating elements in the scale and the remaining coating: (1) the outward diffusion of Ti, Si, and Al atoms to form their oxides in the scale and (2) the inward diffusion of Si and Al into the substrate driveled by the concentration gradient. The outward diffusion of Si and Al is beneficial to the anti-oxidation performance of the scale by forming protective SiO_2 and Al_2O_3. However, the outward diffusion of Ti is considered detrimental because the TiO_2 scale formed during high-temperature oxidation cannot provide long-term oxidation protection due to its porous structure [4]. This is different from the TiO_2 scales produced by anodic oxidation and passivation, which have been proven to be dense and compact [47]. It is noted that the $TiAl_2$ inner layer in the Si-Co diffusion coating (Figure 2b) can act as an important Al resource for the formation of Al_2O_3 in the scale through outward diffusion, and simultaneously, it can also act as a barrier for the inward diffusion of Si because the solid solubility of Si in $TiAl_2$ is generally lower than 0.3 at.% [43]. Thus, the formation of the $TiAl_2$ inner layer should be very beneficial for the anti-oxidation performance of the coating.

4. Conclusions

By optimizing proper co-deposition temperature and pack Co content, a dense Si-Co diffusion coating can be obtained on TiAl-Nb alloys. The coating had a typical structure of a (Ti,*X*)Si_2+Ti_5Si_4 (*X* represents Nb and Al elements) outer layer with a Co-rich superficial zone, a Ti_5Si_4+Ti_5Si_3 middle layer, and a $TiAl_2$ inner layer. Increasing the co-deposition temperature in the range of 1050–1120 °C led to a larger coating thickness but a more-porous coating structure, while increasing the pack Co contents in the range of 5–20 wt.% caused a lower coating growth rate. Moreover, the formation of the Si-Co diffusion coatings on the TiAl-Nb alloy followed an orderly process of depositing Si first and then Co, during which the inward reaction diffusion of Si in the substrate was the dominant factor for the growth of the coatings.

The Si-Co diffusion coating had much better anti-oxidation properties than both the TiAl-Nb substrate and pure silicide coating. After oxidation at 1000 °C for 100 h, the scale consisted of SiO_2, TiO_2, and Al_2O_3 mixtures formed on the surface of the Si-Co diffusion coating, which can offer effective protection for the base alloy from oxidation. The oxidation parabolic rate of the Si-Co diffusion coating was about 6.16×10^{-3} mg^2/cm^4h^1, lower than those of the TiAl-Nb substrate by about two orders of magnitude and pure silicide coating by about one order of magnitude.

Author Contributions: All authors contributed to the study conception and design. Material preparation, data collection and analysis were performed by J.T., W.L. and X.L. The first draft of the manuscript was written by J.T., and amended by C.Z. and W.T. All authors commented on previous versions of the manuscript. All authors have read and agreed to the published version of the manuscript.

Funding: This research was financially supported by the Innovation Capacity Support Plan Project of Shanxi Province (No. 2020GHJD-10), the Young Science and Technology Rising Star Project of Shanxi Province (No. 2021KJXX-79), the Science and Technology Plan Project of Sichuan Province (No. 2022YFSY0036).

Institutional Review Board Statement: Not applicable.

Informed Consent Statement: Not applicable.

Data Availability Statement: Not applicable.

Conflicts of Interest: The authors declare no conflict of interest.

References

1. Duan, B.H.; Yang, Y.C.; He, S.Y.; Feng, Q.S.; Mao, L.; Zhang, X.X.; Jiao, L.N.; Lu, X.G.; Chen, G.Y.; Li, C.H. History and development of γ-TiAl alloys and the effect of alloying elements on their phase transformations. *J. Alloys Compd.* **2022**, *909*, 164811. [CrossRef]
2. Kim, S.W.; Hong, J.K.; Na, Y.S.; Yeom, J.T.; Kim, S.E. Development of TiAl alloys with excellent mechanical properties and oxidation resistance. *Mater. Des.* **2014**, *54*, 814–819. [CrossRef]
3. Banumathy, S.; Neelam, N.S.; Chandravanshi, V.; Bhattacharjee, A.; Ravi, K.R. The Effect of Nb addition on microstructure, oxidation behavior and strength of some γ-TiAl alloys. *Mater. Today Proc.* **2018**, *5*, 5514–5520. [CrossRef]
4. Lin, J.P.; Zhao, L.L.; Li, G.Y.; Zhang, L.Q.; Song, X.P.; Ye, F.; Chen, G.L. Effect of Nb on oxidation behavior of high Nb containing TiAl alloys. *Intermetallics* **2011**, *19*, 131–136. [CrossRef]
5. Pflumm, R.; Friedle, S.; Schütze, M. Oxidation protection of γ-TiAl-based alloys–a review. *Intermetallics* **2015**, *56*, 1–14. [CrossRef]
6. Zhou, C.G.; Xu, H.B.; Gong, S.K.; Kim, Y. A study of aluminide coatings on TiAl alloys by the pack cementation method. *Mater. Sci. Eng. A* **2003**, *341*, 169–173. [CrossRef]
7. Sasaki, T.; Yagi, T.; Watanabe, T.; Yanagisawa, A. Aluminizing of TiAl-based alloy using thermal spray coating. *Surf. Coat. Technol.* **2011**, *205*, 3900–3904. [CrossRef]
8. Dudziak, T.; Du, H.L.; Datta, P.K.; Wilson, A.; Ross, I.M.; Moser, M.; Braun, R. Sulphidation/oxidation behaviour of TiAlCr and Al_2Au coated Ti45Al8Nb alloy at 750 °C. *Corros. Sci.* **2009**, *51*, 1189–1196. [CrossRef]
9. Braun, R.; Kelm, K.; Fröhlich, M.; Leyens, C. Oxidation resistance of γ-TiAl based alloy Ti–45Al–8Nb coated with intermetallic Ti–Al–Cr–Y layers and EB-PVD zirconia topcoats at 950 °C in air. *Surf. Coat. Technol.* **2013**, *222*, 128–134. [CrossRef]
10. Han, D.; Liu, D.; Niu, Y.; Qi, Z.; Pan, Y.; Xu, H.; Zheng, X.; Chen, G. Interface stability of NiCrAlY coating without and with a Cr or Mo diffusion barrier on Ti-42Al-5Mn alloy. *Corros. Sci.* **2021**, *188*, 109538. [CrossRef]
11. Dudziak, T.; Datta, P.K.; Mayrhofer, P.H.; Rovere, F. High Temperature Oxidation Resistance of CrAlYN-Coated Ti45Al8Nb. *Oxid. Met.* **2011**, *75*, 359–376. [CrossRef]
12. Wang, S.Q.; Xie, F.Q.; Wu, X.Q.; Chen, L.Y. CeO_2 doped Al_2O_3 composite ceramic coatings fabricated on γ–TiAl alloys via cathodic plasma electrolytic deposition. *J. Alloys Compd.* **2019**, *788*, 632–638. [CrossRef]
13. Wu, L.K.; Xia, J.J.; Cao, H.Z.; Liu, W.J.; Hou, G.Y.; Tang, Y.P.; Zheng, G.Q. Improving the high-temperature oxidation resistance of TiAl alloy by anodizing in Methanol/NaF solution. *Oxid. Met.* **2018**, *90*, 617–631. [CrossRef]
14. Yao, J.; He, Y.; Wang, D.; Lin, J. High-temperature oxidation resistance of (Al_2O_3–Y_2O_3)/(Y_2O_3-stabilized ZrO_2) laminated coating on 8Nb–TiAl alloy prepared by a novel spray pyrolysis. *Corros. Sci.* **2014**, *80*, 19–27. [CrossRef]
15. Ma, X.; He, Y.; Lin, J.; Wang, D.; Zhang, J. Effect of a magnetron sputtered (Al_2O_3–Y_2O_3)/(Pt–Au) laminated coating on hot corrosion resistance of 8Nb–TiAl alloy. *Surf. Coat. Technol.* **2012**, *206*, 2690–2697. [CrossRef]
16. Cockeram, B.V.; Rapp, R.A. The kinetics of multilayered titanium-silicide coatings grown by the pack cementation method. *Metall. Mater. Trans. A* **1995**, *26*, 777–791. [CrossRef]
17. Huang, J.; Zhao, F.; Cui, X.; Wang, J.; Xiong, T. Long-term oxidation behavior of silicon-aluminizing coating with an in-situ formed Ti_5Si_3 diffusion barrier on γ-TiAl alloy. *Appl. Surf. Sci.* **2022**, *582*, 152444.
18. Mitra, R. Mechanical behaviour and oxidation resistance of structural silicides. *Int. Mater. Rev.* **2006**, *51*, 13–64. [CrossRef]
19. Xiao, L.; Zhou, X.; Wang, Y.; Pu, R.; Zhao, G.; Shen, Z.; Zhao, X. Formation and oxidation behavior of Ce-modified $MoSi_2$-$NbSi_2$ coating on niobium alloy. *Corros. Sci.* **2020**, *173*, 108751. [CrossRef]
20. Li, H.J.; Feng, T.; Fu, Q.G.; Wu, H.; Shen, X.T. Oxidation and erosion resistance of $MoSi_2$–$CrSi_2$–Si/SiC coated C/C composites in static and aerodynamic oxidation environment. *Carbon* **2010**, *48*, 1636–1642. [CrossRef]
21. Zhu, X.; Zhang, Y.; Qiang, X.; Zhang, J.; Su, Y.; Li, T. An oxidation protective coating prepared by SiC densifying HfB2-SiC skeleton for SiC-coated C/C composites at 1473, 1773, and 1973 K. *Corros. Sci.* **2022**, *207*, 110559. [CrossRef]
22. Liu, Y.; Hu, R.; Yang, J.; Li, J. Tensile properties and fracture behavior of in-situ synthesized Ti2AlN/Ti48Al2Cr2Nb composites at room and elevated temperatures. *Mat. Sci. Eng. A* **2017**, *679*, 7–13. [CrossRef]
23. Zhang, L.; Wu, J. Thermal expansion and elastic moduli of the silicide based intermetallic alloys Ti_5Si_3 (X) and Nb_5Si_3. *Scr. Mater.* **1997**, *38*, 307–313. [CrossRef]
24. Xiang, Z.D.; Rose, S.R.; Datta, P.K. Codeposition of Al and Si to form oxidation-resistant coatings on γ-TiAl by the pack cementation process. *Mater. Chem. Phys.* **2003**, *80*, 482–489. [CrossRef]
25. Yu, W.H.; Tian, J.; Tian, W.; Zhao, J.; Li, Y.; Liu, Y. Study of yttrium and cerium on the oxidation resistance of silicide coatings prepared on Ti-6Al-4V alloy by pack-cementation process. *J. Rare Earth* **2015**, *33*, 221–226. [CrossRef]
26. Koo, C.H.; Yu, T.H. Pack cementation coatings on Ti_3Al–Nb alloys to modify the high-temperature oxidation properties. *Surf. Coat. Technol.* **2000**, *126*, 171–180. [CrossRef]
27. Semenov, N.A. Oxidation resistance of niobium coated with titanium disilicide. *Powder Metall. Met. Ceram.* **2000**, *39*, 560–562. [CrossRef]
28. Bai, C.Y.; Luo, Y.J.; Koo, C.H. Improvement of high temperature oxidation and corrosion resistance of superalloy IN-738LC by pack cementation. *Surf. Coat. Technol.* **2004**, *183*, 74–88. [CrossRef]
29. Strydom, W.J.; Lombaard, J.C.; Pretorius, R. Thermal oxidation of the silicides $CoSi_2$, $CrSi_2$, $NiSi_2$, PtSi, $TiSi_2$ and $ZrSi_2$. *Thin Solid Films* **1985**, *131*, 215–231. [CrossRef]
30. Becker, S.; Rahmel, A.; Schütze, M. Oxidation of $TiSi_2$ and $MoSi_2$. *Solid State Ionics* **1992**, *53*, 280–289. [CrossRef]

31. Qiao, M.; Zhou, C.G. Co-deposition of Co–Al–Y on nickel base superalloys by pack cementation process. *Corros. Sci.* **2013**, *75*, 454–460.
32. Zamoum, F.; Benlaharche, T.; David, N.; Podor, R.; Vilasi, M. Kinetics of high temperature oxidation of $(Nb,Co,Cr)_7Si_6$ and $(Nb,Co,Cr)_8Si_7$ silicide compounds. *Intermetallics* **2008**, *16*, 498–507. [CrossRef]
33. Thanneeru, R.; Patil, S.; Deshpande, S.; Seal, S. Effect of trivalent rare earth dopants in nanocrystalline ceria coatings for high-temperature oxidation resistance. *Acta Mater.* **2007**, *55*, 3457–3466.
34. Zhao, L.L.; Li, G.Y.; Zhang, L.Q.; Lin, J.P.; Song, X.P.; Ye, F.; Chen, G.L. Influence of Y addition on the long time oxidation behaviors of high Nb containing TiAl alloys at 900 °C. *Intermetallics* **2010**, *18*, 1586–1596. [CrossRef]
35. Qu, S.J.; Tang, S.Q.; Feng, A.H.; Feng, C.; Shen, J.; Chen, D.L. Microstructural evolution and high-temperature oxidation mechanisms of a titanium aluminide based alloy. *Acta Mater.* **2018**, *148*, 300–310. [CrossRef]
36. Bianco, R.; Rapp, R.A.; Jacobson, N.S. Volatile species in halide-activated diffusion coating packs. *Oxid. Met.* **1992**, *38*, 33–43.
37. Tian, J.; Zhang, C.; Li, X.; Lai, S.; Xie, W.L.; Tian, W. Wear Behavior of Silicon-Cobalt Composite Coating Deposited on TiAl Alloy by Pack Cementation Process. *J. Mater. Eng. Perform.* **2022**, *31*, 4811–4819. [CrossRef]
38. Xiang, L.L.; Zhao, L.L.; Wang, Y.L.; Zhang, L.Q.; Lin, J.P. Synergistic effect of Y and Nb on the high temperature oxidation resistance of high Nb containing TiAl alloys. *Intermetallics* **2012**, *27*, 6–13.
39. Yamane, T.; Fujiishi, Y.; Araki, H.; Minamino, Y.; Saji, S.; Takahashi, J.; Miyamoto, Y. Phase diagrams of the Ti-Si system under high pressure. *J. Mater. Sci. Lett.* **1994**, *13*, 200–202.
40. Falke, M.; Gebhardt, B.; Beddies, G.; Teichert, S.; Hinneberg, H.J. Epitaxial $CoSi_2$ by solid phase reaction of Co/Ti and Co/Hf bilayers on Si(001). *Microelectron. Eng.* **2001**, *55*, 171–175.
41. Chen, G.L.; Wang, X.T.; Ni, K.Q.; Hao, S.M.; Cao, J.X.; Ding, J.J.; Zhang, X. Investigation on the 1000, 1150 and 1400 °C isothermal section of the TiAlNb system. *Intermetallics* **1996**, *4*, 13–22. [CrossRef]
42. Pang, X.Z.; Chen, X.; Yang, J.; Pang, M.; Yang, W.; Zhan, Y. Influence of Nb concentration on the structure, stability, and electronic and mechanical properties of D022 Al3Ti by first-principles calculations and experiments. *J. Phys. Chem. Solids* **2019**, *131*, 243–253. [CrossRef]
43. Kahrobaee, Z.; Palm, M. Experimental investigation of Ti–Al–Si phase equilibria at 800–1200 °C. *J. Alloys Compd.* **2022**, *924*, 166223.
44. Kung, S.C.; Rapp, R.A. Analyses of the gaseous species in halide-activated cementation coating packs. *Oxid. Met.* **1989**, *32*, 89–109.
45. Xiang, Z.D.; Datta, P.K. Relationship between pack chemistry and aluminide coating formation for low-temperature aluminisation of alloy steels. *Acta Mater.* **2006**, *54*, 4453–4463.
46. Krendelsberger, N.; Weitzer, F.; Schuster, J.C.; Stein, F. Constitution of the ternary system Co–Si–Ti. *Intermetallics* **2013**, *38*, 92–101. [CrossRef]
47. Sahu, B.P.; Ray, M.; Mitra, R. Structure and properties of $Ni_{1-x}Ti_xN$ thin films processed by reactive magnetron co-sputtering. *Mater. Charact.* **2020**, *169*, 110604.

Disclaimer/Publisher's Note: The statements, opinions and data contained in all publications are solely those of the individual author(s) and contributor(s) and not of MDPI and/or the editor(s). MDPI and/or the editor(s) disclaim responsibility for any injury to people or property resulting from any ideas, methods, instructions or products referred to in the content.